



HAL
open science

A STUDY OF THE $\alpha \leftrightarrow \gamma$ TRANSFORMATION IN PURE IRON: RATE VARIATIONS REVEALED BY MEANS OF THERMAL ANALYSIS

Claudia Papandrea, Livio Battezzati

► **To cite this version:**

Claudia Papandrea, Livio Battezzati. A STUDY OF THE $\alpha \leftrightarrow \gamma$ TRANSFORMATION IN PURE IRON: RATE VARIATIONS REVEALED BY MEANS OF THERMAL ANALYSIS. Philosophical Magazine, 2007, 87 (10), pp.1601-1618. 10.1080/14786430601080260 . hal-00513807

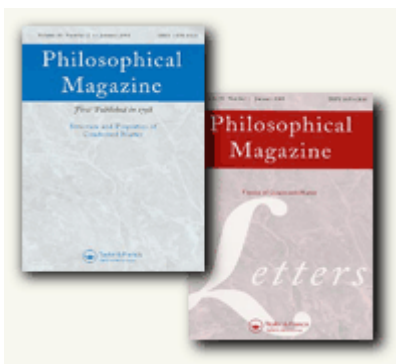
HAL Id: hal-00513807

<https://hal.science/hal-00513807>

Submitted on 1 Sep 2010

HAL is a multi-disciplinary open access archive for the deposit and dissemination of scientific research documents, whether they are published or not. The documents may come from teaching and research institutions in France or abroad, or from public or private research centers.

L'archive ouverte pluridisciplinaire **HAL**, est destinée au dépôt et à la diffusion de documents scientifiques de niveau recherche, publiés ou non, émanant des établissements d'enseignement et de recherche français ou étrangers, des laboratoires publics ou privés.



**A STUDY OF THE $\alpha \leftrightarrow \gamma$ TRANSFORMATION IN PURE IRON:
RATE VARIATIONS REVEALED BY MEANS OF THERMAL
ANALYSIS**

Journal:	<i>Philosophical Magazine & Philosophical Magazine Letters</i>
Manuscript ID:	TPHM-06-Sep-0356
Journal Selection:	Philosophical Magazine
Date Submitted by the Author:	07-Sep-2006
Complete List of Authors:	Papandrea, Claudia; Università di Torino, Dipartimento di Chimica Ifm e Centro NIS Battezzati, Livio; Università di Torino, Dipartimento di Chimica Ifm e Centro NIS
Keywords:	phase transformations, DTA
Keywords (user supplied):	Iron, Interface migration



A STUDY OF THE $\alpha \leftrightarrow \gamma$ TRANSFORMATION IN PURE IRON: RATE VARIATIONS REVEALED BY MEANS OF THERMAL ANALYSIS

Claudia Papandrea and Livio Battezzati*

Dipartimento di Chimica IFM e NIS-Centro di Eccellenza, Università di Torino,
Via P. Giuria 7, 10125 Torino, Italy

*Corresponding author: tel + 39 011 6707567; fax + 39 011 6707855, e-mail:
livio.battezzati@unito.it

Abstract

The $\alpha \leftrightarrow \gamma$ transformation in nominally high purity Fe is shown to occur with a stepped peak in differential thermal analysis on both heating and cooling at rates between 0.5 Kmin^{-1} and 10 Kmin^{-1} . The composite peaks mark changes in the transformation rate. To endorse the findings, the instrumental output has been thoroughly analysed providing evaluations of time lags, suggestions for calibration and for the use of the derivative of the peak.

The change in rate occurred in all sampled irrespective of their grain size (average values from $91 \mu\text{m}$ to $1100 \mu\text{m}$). The rate of movement of the interface in the $\alpha \leftrightarrow \gamma$ transformation is estimated in between $4 \cdot 10^{-5} \text{ ms}^{-1}$ and $3 \cdot 10^{-6} \text{ ms}^{-1}$. The present results extend previous dilatometric work in which the rate variation was detected only for large grain size and low undercooling.

Possible reasons for the variation in rate are outlined: local development of strain in the austenite due to lattice misfit with respect of the growing ferrite, formation of a ragged microstructure, pinning of the boundaries by impurity.

Keywords

Iron, massive phase transformation, interface migration, differential thermal analysis.

1. Introduction

During the last decade there has been continuous interest in experimental and theoretical studies on the $\alpha \leftrightarrow \gamma$ transformation in Fe and Fe alloys due to its relevance in steel processing [1-11]. Papers have appeared in relation to the kinetics of such transformation [1, 3, 4], the topology of grains [2], the mobility of the interface between the two phases, dilatation and enthalpic effects. Dilatometry is often employed for the monitoring of the transformation on cooling, the kinetics of which is modelled according to a nucleation and growth mechanism [3, 5]. An amount of undercooling is always reported for the start of the transformation. Assuming instantaneous nucleation at the undercooling temperature, the growth of ferrite was analysed for a series of Fe alloys containing up to 2 at% of Co, Cu, Mn, Cr, Al, and the molar mobility of the interface, M , was obtained as $2.4 \cdot \exp(-140000/RT) \text{ mol} \cdot \text{m} \cdot (\text{J} \cdot \text{s})^{-1}$ when the impurity nitrogen content was below 40 ppm. It decreased about an order of magnitude for an order of magnitude increase in nitrogen content [4]. The mobility is related to the interface velocity, v , by

$$v = M \cdot \Delta G_m \quad (1)$$

where ΔG_m is the driving force per mole. Since the driving force is of the order of 10 - $100 \text{ J} \cdot \text{mol}^{-1}$ at the given undercoolings [1, 6], the interface velocity, v , is estimated in the range from 10^{-4} to 10^{-6} ms^{-1} . Direct observation of the interface movement in a low C and low N steel provided values of v from $1 \cdot 10^{-4} \text{ ms}^{-1}$ to $9 \cdot 10^{-4} \text{ ms}^{-1}$ [7].

Differential thermal analysis (DTA) has been employed to obtain the transformed fraction of ferrite as a function of heating rate in Fe-1at%Mn and Fe-2at%Mn steels. From the subsequent kinetic analysis, interface velocities from 0.2 to $0.9 \cdot 10^{-6} \text{ ms}^{-1}$ were calculated [1]. Further analyses

1
2
3 with a Fe-1.89at%Mn steel showed that the transformation occurs in two stages the velocities of
4
5 which fall in the range just reported [8].
6
7

8 By performing both isochronal dilatometric and differential thermal analyses, the $\gamma \rightarrow \alpha$
9
10 transformation was found to occur either normally or abnormally in Fe-Co, Fe-Mn and pure Fe
11
12 according to the grain size in the sample [6, 9]. With grains of the order of tens of micrometers
13
14 (alloys) or 273-372 μm (pure Fe), a single step transformation was detected (normal behaviour),
15
16 whereas up to three steps were detected when the grains were 439 μm (abnormal behaviour). The
17
18 steps have been related to variations of the formation rate of ferrite and have been detected during
19
20 cooling. As for the reverse $\alpha \rightarrow \gamma$ transformation, no detailed analysis was apparently performed with
21
22 either technique. It was, anyway, shown that the abnormal behaviour could be revealed by means of
23
24 DTA isothermal analyses at temperatures very close to the equilibrium one. From the kinetic
25
26 modelling of the dilatometric results, the interface velocities for the normal transformation were
27
28 derived as $2\cdot 3\cdot 10^{-7} \text{ m}\cdot\text{s}^{-1}$ for Fe-2.26 at%Mn, $4\cdot 8\cdot 10^{-6} \text{ m}\cdot\text{s}^{-1}$ for Fe-1.79 at%Co and $3\cdot 6\cdot 10^{-6} \text{ m}\cdot\text{s}^{-1}$ for
29
30 pure Fe [6, 10]. The interface velocities for the abnormal transformation were in excess of $2\cdot 10^{-4}$
31
32 ms^{-1} [6]. In these studies the $\gamma \rightarrow \alpha$ transformation in substitutional alloys was considered as a
33
34 partitionless transformation in view of the slow diffusion of substitutional elements in Fe [9].
35
36
37
38
39
40

41 The topic of interface mobility has been recently reviewed by comparing all data available in the
42
43 literature and concluding that the scatter of data is still very large and more work is needed to
44
45 elucidate the effect of grain size, impurity content, number of transformation steps [11].
46
47
48

49 A further point of discussion refers to the technique employed to follow the transformation.
50
51 Dilatometry appears more straightforward in that the length change is immediately detected by a
52
53 transducer although the accuracy of the temperature control of the sample can be limited due to its
54
55 size and position in the measuring device (e. g. it is within 10 K when the instrument is operated at
56
57 the heating/cooling rate of 20 Kmin^{-1} [5]). DTA, instead, provides much better control of the sample
58
59 temperature whereas the heat effect due to the transformation can be smeared due to instrumental
60
thermal lag [12].

1
2
3 The interest in the topic arose from the need of a careful instrumental calibration and interpretation
4 of DTA results obtained with various industrial alloys as a ground support for further studies to be
5 performed in microgravity [13]. This paper reports an analysis of the $\alpha \leftrightarrow \gamma$ transformation in
6 nominally pure Fe by DTA with attention to the occurrence of the transformation on heating which
7 was not studied either by dilatometry and thermal analysis in previous works. This is preceded and
8 accompanied by a discussion on the calibration of the instrument and on the interpretation of the
9 signal given by first order transformations by comparing the $\alpha \leftrightarrow \gamma$ transformation of Fe with the
10 melting of pure elements and the $\alpha \leftrightarrow \beta$ transformation of Ti.
11
12
13
14
15
16
17
18
19
20
21
22
23
24

25 2. Experimental

26
27
28
29
30 Iron samples for thermal analysis were cut from a rod of 4 mm in diameter at various length
31 in order to have sample masses from 250 mg to 2000 mg. The purity was 99.98% (Sigma Aldrich,
32 product no. 266213) and the metal impurity content was detailed by the producer as 2.5 ppm Ti and
33 0.7 ppm Cu. Rolled foils were also used, made of a laboratory refined iron, with sample masses
34 from 130 mg to 440 mg. The metal impurity content, determined by neutron activation, was (all
35 values in ppm): Cu 3, Mo 2, Co 1, Mn 1, Ni 1, Cr 0.4, traces of W, Ag, Zn were detected.
36
37
38
39
40
41
42
43

44 Thermal analysis was performed with the high temperature differential scanning calorimeter
45 of Setaram. The cell is made of alumina and the sample is contained in an alumina pan with some
46 alumina powder to prevent it from sticking to the crucible walls. The sensor for the sample and
47 reference cell is a thermopile and the instrumental output is a temperature difference. Therefore, the
48 instrument will be referred to as a differential thermal analyser (DTA) The cell is evacuated and
49 purged several times before measuring under flowing Helium filtered to remove residual oxygen
50 and water vapour. The standard thermal cycle was as follows. The specimen was heated from room
51 temperature to 893 K at the rate of 15 Kmin⁻¹ and kept at this temperature for 30 min. Then it was
52 heated at the rate of 10 Kmin⁻¹ to 1293 K and kept at this temperature for 30 min. At last it was
53
54
55
56
57
58
59
60

1
2
3 cooled at the rate of -10 Kmin^{-1} to 893 K and kept at this temperature for 30 min. For the various
4
5 samples iron, one or more cycles reported before, have been performed. Various experiments were
6
7 performed also at the rates of 0.1, 0.5, 2, 5 Kmin^{-1} . The DTA cell was calibrated for the temperature
8
9 and the heat flow by recording the melting temperature and heat of fusion of various pure metal
10
11 samples (Al, Ag, Au, Cu, Ni) at the rates of 2, 5, and 10 Kmin^{-1} . The frequency of sampling of the
12
13 data points was one point every 1 to 3 s according to the heating or cooling rate for a total of 4800
14
15 point per file.
16
17
18

19
20 The microstructure of the samples was observed before and after thermal cycles by optical
21
22 microscopy. The ferrite grain boundaries were revealed by etching with 1.5 vol.% Nital solution.
23
24 The average grain size was determined with the intercept method.
25
26
27
28

29 **3. Results and Discussion**

30 31 32 33 34 *3.1. The shape of the signal and the temperature calibration of DTA: Curie point of Fe versus* 35 36 *melting of Au* 37 38 39 40

41 The molar heat capacity of seven samples of pure Fe has been determined on both heating
42
43 and cooling at the rate of 10 Kmin^{-1} in the temperature range from 950 K to 1100 K. The results
44
45 obtained after calibrating the temperature of the instrument with the melting point of various metals
46
47 on heating, are reported in Figs. 1 and 2, respectively. On heating the specific heat increases up to
48
49 the ferro- to para-magnetic transition, T_c , and then drops steadily (Fig. 1). The present data are in
50
51 good agreement with those reported in [12]. The figures also contain the C_p of Fe as computed as a
52
53 function of temperature from assessed empirical equations: the one proposed by the Scientific
54
55 Group Thermodata Europe (SGTE) (thin full curve) and widely employed for establishing lattice
56
57 stability in phase diagram assessments, that suggested in [12] (dotted line) which uses parameters
58
59 accounting for all the data available in the literature for the magnetic contribution to the specific
60

1
2
3 heat of Fe in addition to those from SGTE, and that obtained in the most recent modelling of
4 thermodynamic properties of Fe by careful consideration of both ferro- and para-magnetic
5 contributions to the specific heat [15]. There is general agreement of data, apart from the
6 temperature region of the transition where experiments provide a more pronounced cusp with
7 respect to models.
8
9

10
11 On cooling, the specific heat increases on approaching the Curie point but the cusp is not as sharp
12 as on heating. The maximum of the curve occurs at lower temperature with respect to the assessed
13 T_c which apparently coincides with the onset of the C_p rise. These observations were already made
14 in [12] and led to the de-smearing procedure described in that paper. With this procedure, the
15 experimental curves were shifted and corrected so that they coincided on both heating and cooling.
16
17 However, a procedure for the use of the Curie temperature as a calibration point on cooling was not
18 given. This is desirable since the solidification of metals mostly occurs with some undercooling
19 and, therefore, there is no suggested substance for such calibration in the temperature range
20 considered here, but only for lower temperatures [16]. If it is evident that the C_p cusp at T_c on
21 heating is well suited for calibrating the cell by running it at various rates, the smeared curve on
22 cooling does not provide an immediate indication. In fact, only after de-smearing the C_p curve
23 presents a discontinuity at the Curie point on cooling [12]. For as-recorded traces in the absence of
24 temperature calibration, the choice is left between the maximum of the curve and the onset of its
25 rise (Fig. 2).
26
27
28
29
30
31
32
33
34
35
36
37
38
39
40
41
42
43
44
45
46
47

48 In this work the Curie point of Fe samples and the melting and solidification point of Au
49 samples were obtained as a function of heating and cooling rates in a set of experiments performed
50 before the temperature of the instrument was calibrated. As expected [17], transformations points
51 scaled with the heating rate. The melting and solidification points of Au were chosen among those
52 available for various metals (Al, Ag, Au, Cu, Ni) because the transformation on cooling occurred
53 with very limited undercooling, often practically undetectable with our experimental set up.
54 Examples of DTA traces for melting and solidification of Au are shown, together with their
55
56
57
58
59
60

derivative, in Fig. 3 and 4, respectively. They are discussed here, in the context of calibration but the conclusions will be useful for the general interpretation of the DTA signal given by thermodynamic first order transformations.

The DTA trace for the melting of Au (Fig. 3a) has a slightly smeared onset which is usually attributed to inevitable occasional impurities and continues with a linear trend. When melting is over, the trace decays exponentially towards the baseline*. The transformation is finished at the minimum of the curve and the transformed fraction is represented by this part of the trace. The full peak should be considered only for integration to get the enthalpy of transformation. The linear part marks the departure of the reference cell temperature which follow the imposed temperature program from that of the sample cell which remains at the melting temperature of the element. This is better illustrated by the derivative of the trace (Fig. 3b) which departs from zero at the melting onset and displays a plateau after a transient time. The end of melting is signalled by the rapid variation in the derivative. The transient time depends on heating rate and the amount of heat to be supplied. On cooling the peak is reversed (Fig. 4a) with a linear part corresponding to the progress of solidification and an exponential return to the baseline.

The difference in temperature, ΔT , between the sample and the reference cell during melting can be expressed as [20]

$$\Delta T = \Phi(t - t_i) + \Delta C \Phi R \quad (2)$$

where t is the time, t_i the onset time of the peak, ΔC the difference in heat capacity between the phases in the sample (here liquid and crystal). Φ the heating rate, and R the heat resistance of the instrument. After melting is complete at t_p , ΔT is given by

* The equations describing the DTA signal have been reported and thoroughly discussed in [18-20].

$$\Delta T = [\Phi(t_p - t_i) + \Delta C \Phi R] \exp[-(t - t_p) / \tau] \quad (3)$$

where τ is the time constant for temperature equilibration between the sample and reference cells.

ΔC is computed from known specific heats and the sample mass. The quantity R was determined by means of heat flow calibration of the instrument and ΔT computed for $t = t_p$. Taking the relevant times, t_p and t_i , from the DTA trace, the time constant, τ , was determined as 27.5 s.

The derivative of the trace (Fig. 4b) displays again a plateau after a transient time which is shorter than that obtained on heating. Since heat is being evolved by the sample, the temperatures of the sample and reference cells diverge. The transient period measures the instrumental time lag for reaching the steady state of the process. It amounts to about 12 s. The shape of the derivative curve is also indicative of the fact that almost no undercooling has occurred. In fact, in the presence of undercooling the heat release would be immediate and the derivative curve would present no plateau but would contain mostly an abrupt step and a long return to the baseline (insert in Fig. 4b).

Having firmly established the parameters which determine the shape of the signal, we consider the Curie point of Fe samples and the melting and solidification point of Au as a function of heating and cooling rates as obtained in the absence of temperature calibration of the instrument. The deviation of the transformation temperature from the assessed value, ΔT , is reported in Fig. 5. The points are all aligned on the same straight line if the onset temperature of the specific heat rise due to the Curie transition is taken on cooling. The figure also contains the points corresponding to the maximum of the heat effect for the same transition on cooling. They are clearly misaligned with respect to those obtained on heating. It is concluded that the Curie point can be used for temperature calibration of the DTA cell and that on cooling it must be taken as the onset of the specific heat rise.

On a time base, the distance between the actual maximum of the DSC trace on cooling and T_c is a measure of the time for temperature equilibration between the sample and reference cells after a specific heat jump. The corresponding temperature difference is

$$\Delta T = \Delta C \Phi R \{1 - \exp[-(t - t_c) / \tau]\} \quad (4)$$

where t_c is the time at which the Curie point is reached. With the time constant determined above, the rise of the signal as well as the decay of the curve after T_c on heating are well reproduced.

The analysis of the instrumental parameters performed in this section, will be essential in assessing the results which will be reported in the following.

3.2. The $\alpha \leftrightarrow \gamma$ transformation of Fe by DTA

Various samples of pure Fe were cut from the same bar. One of them was used for metallography in order to determine the grain size which resulted $41 \pm 4 \mu\text{m}$. A second one was heated in the DTA cell up to 1173 K at 10 Kmin^{-1} , i. e. a few degrees below the transformation point and immediately cooled to room temperature. The grain size was now $91 \pm 15 \mu\text{m}$. This is taken as the measure of the grain size of ferrite undergoing transformation to austenite. The DTA traces for the $\alpha \rightarrow \gamma$ and $\gamma \rightarrow \alpha$ transformations are reported in Figs. 6a and 7a, respectively. The traces display an asymmetric peak as in the melting transitions described above with no further discernible feature at the resolution of the drawing. If, however, the derivative is taken through the points (Figs. 6b and 7b), it becomes clear that there is no plateau, contrary to Figs. 4b and 5b; instead, there are steps in the curve after the initial transient and the return to the baseline takes longer. The $\gamma \rightarrow \alpha$ transformation is undercooled about 10 K. The derivative of its trace has the same steps as that obtained on heating, the only difference being the higher peak in the curve due to the faster release of heat on undercooling.

The results reported in Figs. 6 and 7 were reproduced with all samples taken from the same bar using heating and cooling rates ranging from 0.5 Kmin^{-1} to 10 Kmin^{-1} . A further example is given in

1
2
3 Fig. 8 for the heating rate of 2 Kmin^{-1} . Here, the composite nature of the peak is clearly seen both in
4 the DSC trace and in its derivative. Only when the DSC experiment was performed at the heating
5 rate of 0.1 Kmin^{-1} the peak had a symmetric shape. Its duration spanned approximately 1300 s. On
6 cooling at the same rate, the transformation occurred at the undercooling of 8 K and lasted about
7 550 s. Its DTA signal had a composite shape as the one shown in Fig. 8. It is apparent that the
8 transformation is not finished at the minimum or maximum of the curves and that its rate varies as a
9 function of transformed fraction. The enthalpy uptake or release for the $\alpha \leftrightarrow \gamma$ transformation lasts
10 about 30 s for the heating rate of 10 Kmin^{-1} . This is of the same order as the time constant, τ , and
11 definitely longer than the time needed for detection of a heat effect by the instrument. It is,
12 therefore, concluded that the stepped signal found at various rates is due to a phenomenon occurring
13 in the sample although smeared by instrumental effects.

14
15 After a heating and cooling cycle at 10 Kmin^{-1} , the grains size of ferrite was checked and
16 resulted $276 \pm 19 \mu\text{m}$. A few samples were cycled three times through the transformation
17 temperature range and their grain size was monitored after each cycle. The grain size ranged from
18 91 μm to 1100 μm (before the third cycle). In all cases the $\alpha \leftrightarrow \gamma$ transformation occurred with a
19 composite peak which was more clearly resolved on heating than on cooling. A series of cycles was
20 performed with analogous outcome using a sample of iron sliced from the same bar which was
21 rolled in all directions to halve its thickness and reduce the grain size.

22 For further series of measurements a sample of high purity iron from another source (see
23 Experimental Part) was used which confirmed once again the above results.

24 25 26 27 28 29 30 31 32 33 34 35 36 37 38 39 40 41 42 43 44 45 46 47 48 49 50 51 52 53 54 55 56 57 58 59 60

3.3. *The $\alpha \leftrightarrow \beta$ transformation of Ti by DTA*

In the previous paragraphs it has been shown that the derivative of the DTA trace differs for two transformations of thermodynamic first order, i. e. the $\alpha \leftrightarrow \gamma$ transformation of Fe and melting

1
2
3 of Au. The former occurs fully in the solid state whereas the latter involves a liquid phase,
4
5 moreover the enthalpy of transformation differs of an order of magnitude. In order to prove that the
6
7 steps found for the $\alpha \leftrightarrow \gamma$ transformation are not due to instrumental response to a transition
8
9 involving only solid phases, the same experiment has been performed at various rates with samples
10
11 of pure Ti which undergoes an $\alpha \leftrightarrow \beta$ transformation in the solid state at 1155 K. Fig. 9 reports the
12
13 DTA trace obtained on heating at $10 \text{ K} \cdot \text{min}^{-1}$ and its derivative. The DTA trace has apparently a
14
15 wide linear portion as indicated by the length of the plateau in the derivative and the transformation
16
17 ends at the minimum of the curve as shown by the abrupt change in sign of the derivative. The time
18
19 lag of the instrument is close to that already given above.
20
21
22
23

24
25 The result obtained for the $\alpha \leftrightarrow \beta$ transformation of Ti confirms that the peculiar DTA features
26
27 found for the $\alpha \leftrightarrow \gamma$ transformation of Fe are specific to this transformation.
28
29
30
31

32 *3.4. Sample microstructure*

33
34
35
36
37 The microstructure of the ferrite phase of all samples was observed after each DTA run and
38
39 the grain size was determined. In all cases ragged grains or sub-grain boundaries were found as
40
41 shown in Fig. 10 for the average grain sizes of $276 \mu\text{m}$ (a) and $1100 \mu\text{m}$ (b). Next to grains grown
42
43 to large dimension, there are often fine grains apparently recrystallized in a later stage. Similar
44
45 microstructures were reported previously for pure Fe, Fe-Co and Fe-Mn alloys and low carbon steel
46
47 [6, 7, 9]. After one heating and cooling cycle the grain size of ferrite increased from $91 \mu\text{m}$ to 276
48
49 μm and to higher values for more cycles. This should be mainly due to the permanence of the
50
51 sample at high temperature after the $\alpha \leftrightarrow \gamma$ transformation since it has been reported that the grain
52
53 size decreases after the reverse transformation [9]. The ferrite grain size is thought to be
54
55 representative of the average austenite grain size [6] consistent with direct observation through the
56
57 temperature range of transformation [7].
58
59
60

3.5. The rate of the $\alpha \leftrightarrow \gamma$ transformation of Fe

The results illustrated by Figs 6 to 8 show that the rate of the $\alpha \leftrightarrow \gamma$ transformation in nominally pure Fe varies as a function of transformed fraction as already observed by others [6]. The present DTA data do not allow a direct determination of such rate. It has been verified that the time over which the transformation occurs scales linearly with the inverse square root of the heating rate employed for the experiments as expected from consideration of heat resistance models for the DTA instrument [20]. Therefore, the length of the peak is related to the need of either supplying heat to or removing heat from the sample cell. If this occurred at constant rate the peak and its derivative would appear as those due to fusion and solidification of a pure element (Figs. 3 and 4). Since the $\alpha \leftrightarrow \gamma$ transformation peaks are composite in shape, it is deduced that that the rate of heat uptake or emission by the sample is not constant. Only on average the transformation time should be comparable with the time expressing the length of the peak, e. g. 30 s for the heating rate of 10 Kmin^{-1} and 90 s for the heating rate of 2 Kmin^{-1} . The distance over which the transformation occurs must be of the order of the grain size in the samples reported above. Therefore, an average range of transformation rates is estimated by dividing the grain size span (276-1100 μm) for the time span (30-90 s), i. e. the time window in which the anomalies in the transformation rate can be detected. The range is in between $4 \cdot 10^{-5} \text{ ms}^{-1}$ and $3 \cdot 10^{-6} \text{ ms}^{-1}$. These values are representative of the rate of movement of the interface. If the interface would move faster, as expected at the beginning of transformation, the DTA signal would not be affected by any variation being determined by the rate of heat transfer. When the rate of transformation decreases, it becomes comparable to that of heat transfer. Actually, at the heating/cooling rate of 10 Kmin^{-1} the steps in the derivative of the DTA signal are better appreciated on heating than on cooling since in the latter case the transformation occurs in the undercooling regime and is, therefore, faster. At the minimum heating rate used in this work (0.1 Kmin^{-1}), the step was not seen on heating since the heat transfer was slow with respect to

1
2
3 the progress of transformation; on cooling the step in the peak appeared again. The peak started at
4
5 1180 K in the undercooling regime and lasted about 230 s during which heat was spontaneously
6
7 released from metastable austenite and the transformation occurred independently from the heat
8
9 transfer. This finding is in agreement with the one reported in [6] where the $\gamma \rightarrow \alpha$ transformation
10
11 could be followed by DTA in the isothermal mode at a temperature of 1180.7 K. Here the
12
13 composite peak spanned the time of 240 s.
14
15

16
17 Our results, however, show that the change in rate of the $\alpha \leftrightarrow \gamma$ transformation of Fe occurs
18
19 in every sample whereas in [6] it was clearly detected in the dilatometric curve only for an Fe
20
21 sample of large grain size (439 μm), detected in the derivative of the curve for a sample of 372 μm
22
23 and not found for grains sizes of 288 μm and 273 μm . These results refer to cooling curves at rates
24
25 from -5 K/min to -15 K/min. The curves on heating were not commented. The reason for the
26
27 discrepancy cannot be indicated with certainty. We note that the sample of larger grain size of [6]
28
29 undercooled less than the others. Accounting for the findings reported above, this can be crucial in
30
31 detecting the change of transformation rate at the given cooling rates. Moreover, the temperature
32
33 control within the sample used for dilatometry (rod of 5 mm diameter and 10 mm in length) was
34
35 reported to be accurate within 10 K [5] whereas the temperature control is more accurate for the
36
37 small sample used in thermal analysis.
38
39
40
41
42

43
44 The variation in transformation rate can be due to various causes. It was attributed in [6] to a
45
46 variation in nucleation rate after the transformation was halted by the local development of strain in
47
48 the austenite due to lattice misfit with respect of the growing ferrite. One further possibility can be
49
50 the formation of the ragged microstructure which is observed frequently in all samples. The bursts
51
52 of nucleation rate referred to above were suggested to cause local grain refinement and grain
53
54 branching and to induce the presence of sub-grain boundaries [6]. It should also been admitted that,
55
56 although high purity samples were employed in all these analyses, the inevitable impurities they
57
58 contain, including interstitials, can be segregated locally at grain boundaries either as solute atoms
59
60 or even ultra fine precipitates causing pinning of the boundaries during their movement.

1
2
3 The average values of the transformation rate estimated in this work are one order of magnitude
4 lower than the average values reported from direct observation of the frames taken in high
5 temperature microscopy of the transformation in a extra-low carbon steel [7] but fall within the
6 range of those collected in the literature for Fe and Fe-alloys [11]. However, the outcome of the
7 present work is that there is a range of transformation rates and that an absolute value can hardly be
8 determined. Therefore, the mobility of the interface should be checked in every case by careful
9 experimentation. The range of values available to date can provide only an indicative guideline.
10
11
12
13
14
15
16
17
18
19
20
21

22 **4. Conclusions**

23
24
25
26
27 In this work the $\alpha \leftrightarrow \gamma$ transformation in nominally high purity Fe was analysed by DTA on
28 heating and cooling. In all cases it occurred with a stepped peak which has been shown to be due to
29 changes in the transformation rate occurring in the course of the transformation itself. In order to
30 reveal this effect a detailed analysis of the instrumental output has been performed determining the
31 time lag for the detection of the signal and for reaching the steady state of transformation by making
32 use also of the derivative of the peak.
33
34
35
36
37
38
39
40

41 The change in rate occurred in all samples considered in this work irrespective of the grain
42 size which was varied from 91 μm to 1100 μm . The range of rates of movement of the interface
43 between the two phases is estimated in between $4 \cdot 10^{-5} \text{ ms}^{-1}$ and $3 \cdot 10^{-6} \text{ ms}^{-1}$ confirming values
44 previously reported.
45
46
47
48
49

50 Possible reasons for this effect are variation in the rate induced by strain built up ahead of
51 the moving interface, local nucleation bursts, pinning by any inevitable impurity. The
52 microstructural evidence can be found in the formation of ragged grain boundaries.
53
54
55
56
57
58
59
60

Acknowledgement

This work has been performed in the framework of the ESA-Thermolab project "High-Precision Thermophysical Property Data of Liquid Metals for Modelling of Industrial Solidification Processes".

References

1. L. van Leeuwen, S. Vooijs, J. Sietsma, S. van der Zwaag, *Metall. Mater. Trans. A* **25A** 2925 (1997).
2. G. P. Krielaart, S. van der Zwaag, *Mater. Sci. Technol.* **14** 10 (1998).
3. T. A. Kop., I. van Leeuwen, J. Sietsma, S. van der Zwaag, *ISIJ International*, **40** 713 (2000)
4. J. J. Wits, T. A. Kop., I. van Leeuwen, J. Sietsma, S. van der Zwaag, *Mater. Sci. Eng.*, **A283** 234 (2000).
5. T. A. Kop, J. Sietsma, S. van der Zwaag, *J. Mater. Sci.*, **36** 519 (2001).
6. Y. C. Liu, F. Sommer, E. J. Mittemeijer, *Phil. Mag.*, **84** 853 (2004).
7. J. Lee, K. Shibata, K. Asakura, Y. Masumoto, *ISIJ International*, **42** 1135 (2002).
8. A. T. W. Kempen, F. Sommer, E. J. Mittemeijer, *Acta Mater.*, **50**, 2545 (2002).
9. Y. C. Liu, F. Sommer, E. J. Mittemeijer, *Acta Mater.*, **51** 507 (2003).
10. Y. C. Liu, F. Sommer, E. J. Mittemeijer, *Acta Mater.*, **52** 2549 (2004).
11. M. Hillert, L. Höglund, *Scripta Mater.*, **54** 1259 (2006).
12. A. T. W. Kempen, F. Sommer, E. J. Mittemeijer, *Thermochim. Acta*, **383** 21 (2002).
13. R. Aune, L. Battezzati, R. Brooks, I. Egry, H.-J. Fecht, J.-P. Garandet, K. C. Mills, A. Passerone, P. N. Quested, E. Ricci, S. Schneider, S. Seetharaman, R. K. Wunderlich, B. Vinet, *Microgravity Science and Technology*; **15** (1) 7 (2005).
14. A. T. Dinsdale, *Calphad*, **15** 317 (1991).
15. Q. Chen, B. Sundman, *J. Phase Equilibria*, **22** 631 (2001).
16. S. M. Sarge, G.W.H. Höhne, H. K. Cammanga, W. Eysel, E. Gmelin, *Thermochim. Acta*, **361** 1 (2000).
17. R. F. Speyer, *Thermal Analysis of Materials* (Marcel Dekker, New York, 1993).
18. J. Šesták, *Thermal Analysis, part D, Thermophysical Properties of Solids, their Measurement and theoretical Thermal Analysis*. In *Comprehensive Analytical Chemistry*, edited by G. Svehla, vol. XII. (Elsevier, Amsterdam, 1984).
19. W. J. Boettinger, U. R. Kattner, *Metall. Mater. Trans. A*, **33A** 1779 (2002).
20. W. F. Hemminger, S. M. Sarge, *J. Therm. Anal.*, **37** 1455 (1991).

Figure Captions

Fig. 1. The specific heat of Fe as obtained in the present work by high temperature DTA, fully calibrated and operated at the heating rate of 10 Kmin^{-1} in the range from 950 K to 1100 K (bold full curve and error bars) and as computed according to Ref. [12] (dotted curve), Ref. [14] (thin full curve), and Ref. [15] (dashed curve).

Fig. 2. The specific heat of Fe as obtained in the present work by high temperature DTA, fully calibrated and operated at the cooling rate of -10 Kmin^{-1} in the range from 1100 K to 950 K (bold full curve and error bars) and as computed according to Ref. [12] (dotted curve), Ref. [14] (thin full curve), and Ref. [15] (dashed curve).

Fig. 3. a) The DTA trace obtained for the melting of a sample of pure Au used for calibration of the instrument. b) The time derivative of the trace reported in a).

Fig. 4. a) The DTA trace obtained for the solidification of the sample of pure Au used for calibration of the instrument and molten as shown in Fig. 3. The trace was chosen because there is practically no undercooling on solidification. The insert shows a trace for a sample which gave 8 K undercooling. b) The time derivative of the trace reported in a). The insert shows the time derivative of the trace in the insert of a).

Fig. 5. The difference between the recorded and assessed values of the Curie temperature of Fe and the melting or solidification point of Au as a function of the heating and cooling rates used in DTA. For these measurements the temperature scale of the instrument was not calibrated. Stars: melting or solidification points of Au; full circles: T_c of Fe (taken as the onset of C_p rise on cooling); open circles: supposed T_c of Fe (taken as the cusp of C_p curve on cooling).

1
2
3
4
5
6
7
8
9
10
11
12
13
14
15
16
17
18
19
20
21
22
23
24
25
26
27
28
29
30
31
32
33
34
35
36
37
38
39
40
41
42
43
44
45
46
47
48
49
50
51
52
53
54
55
56
57
58
59
60

Fig. 6. a) The DTA trace obtained for the $\alpha \rightarrow \gamma$ transformation of a sample of pure Fe at the heating rate of 10 Kmin^{-1} . b) The time derivative of the trace reported in a).

Fig. 7. a) The DTA trace obtained for the $\gamma \rightarrow \alpha$ transformation of a sample of pure Fe at the cooling rate of -10 Kmin^{-1} . b) The time derivative of the trace reported in a).

Fig. 8. a) The DTA trace obtained for the $\alpha \rightarrow \gamma$ transformation of a sample of pure Fe at the heating rate of 2 Kmin^{-1} . b) The time derivative of the trace reported in a).

Fig. 9. a) The DTA trace obtained for the $\alpha \rightarrow \beta$ transformation of a sample of pure Ti at the heating rate of 10 Kmin^{-1} . b) The time derivative of the trace reported in a).

Fig. 10. a) The microstructure of a sample of pure Fe after one heating and cooling run through the $\alpha \leftrightarrow \gamma$ transformation range. b) The microstructure of a sample of pure Fe after two heating and cooling runs through the $\alpha \leftrightarrow \gamma$ transformation range.

Figure 1

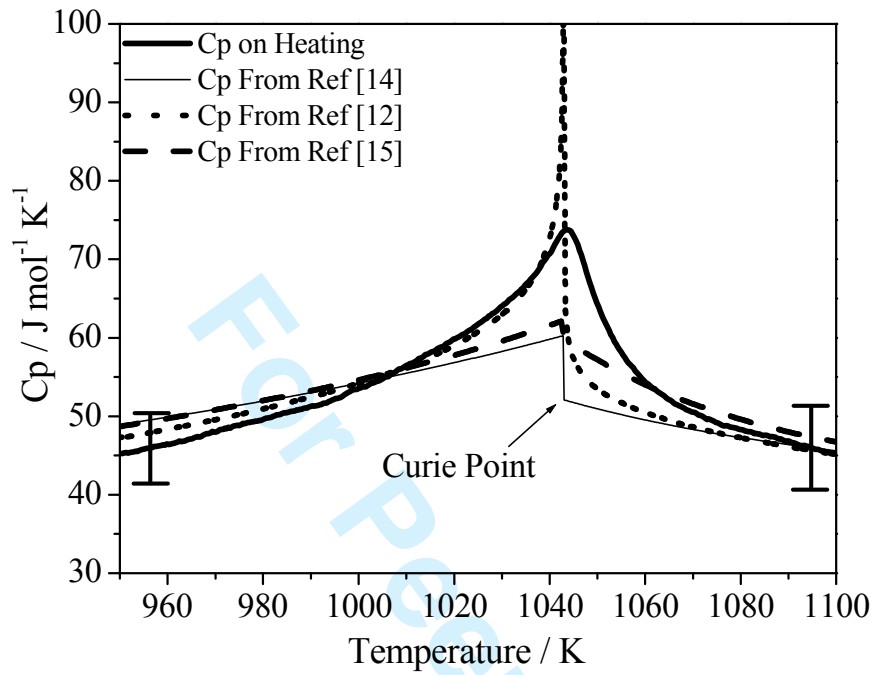


Figure 2

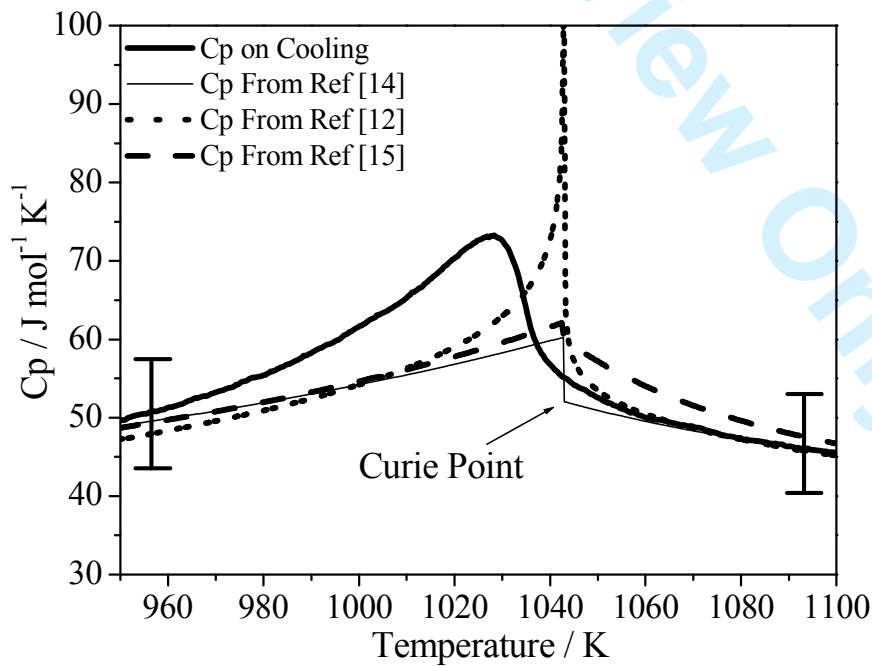


Figure 3a

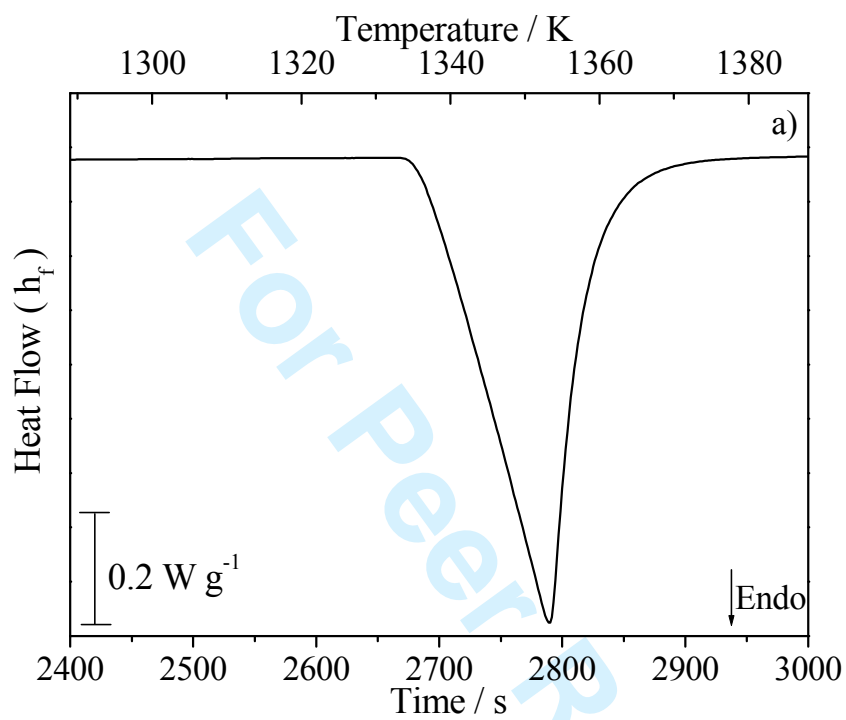


Figure 3b

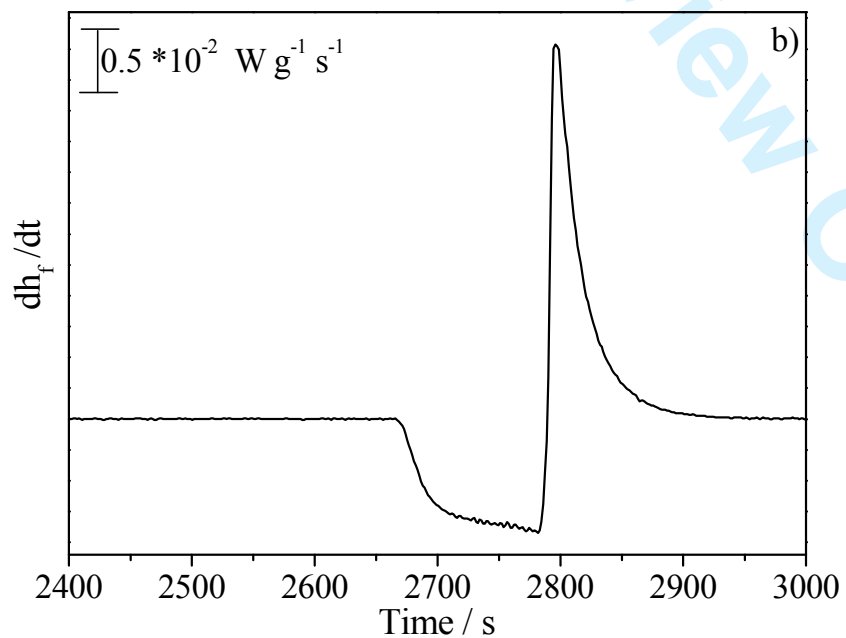


Figure 4a

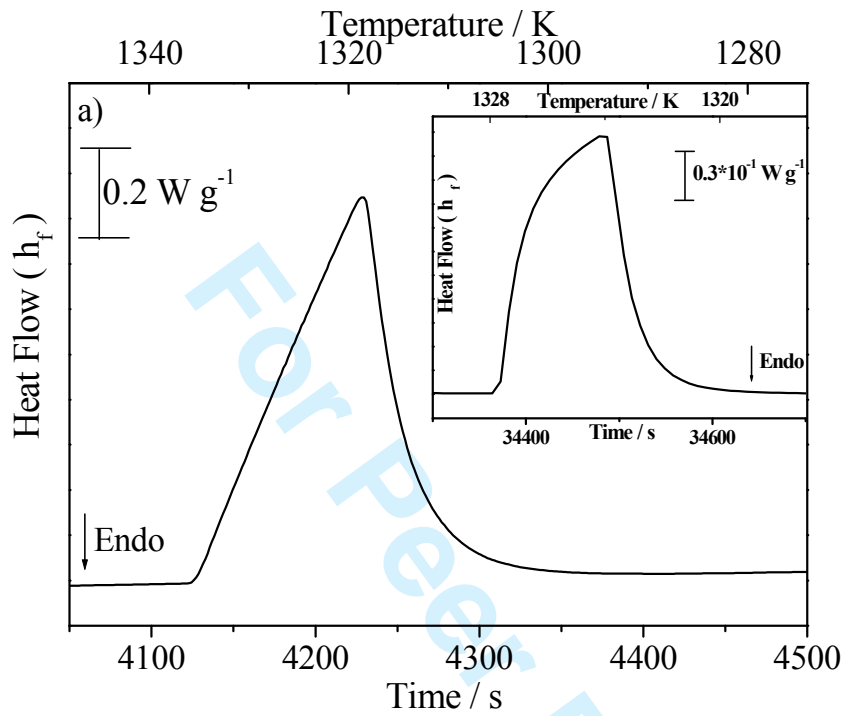


Figure 4b

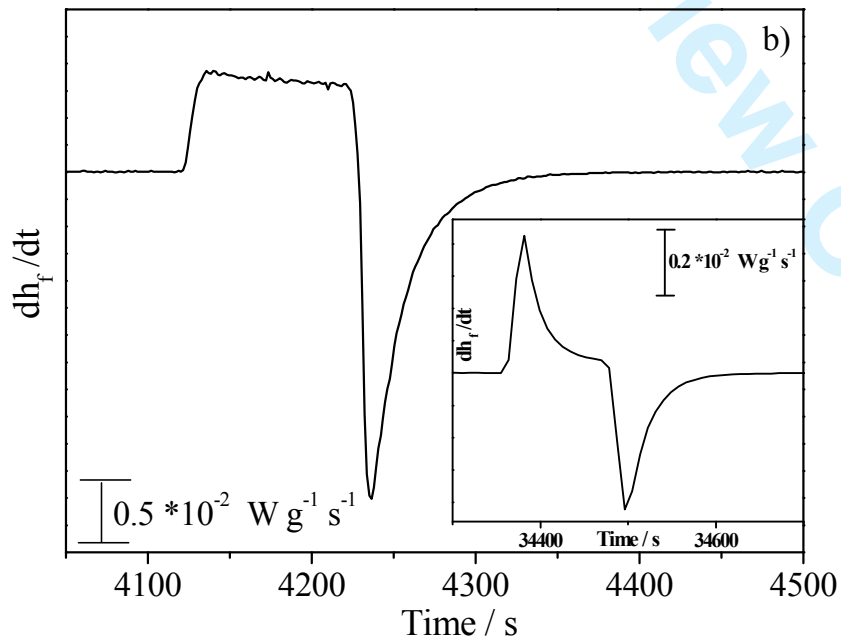


Figure 5

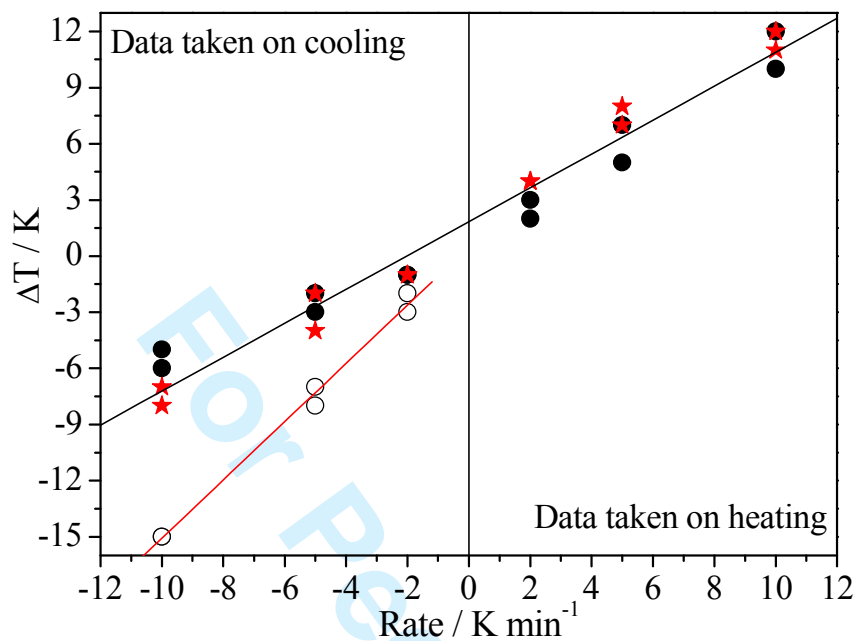


Figure 6a

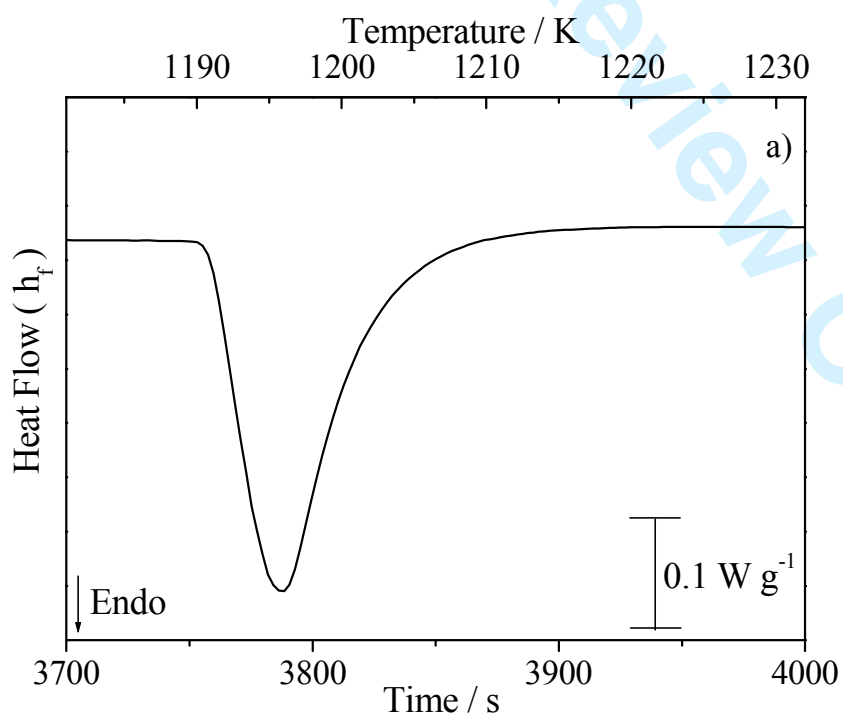


Figure 6b

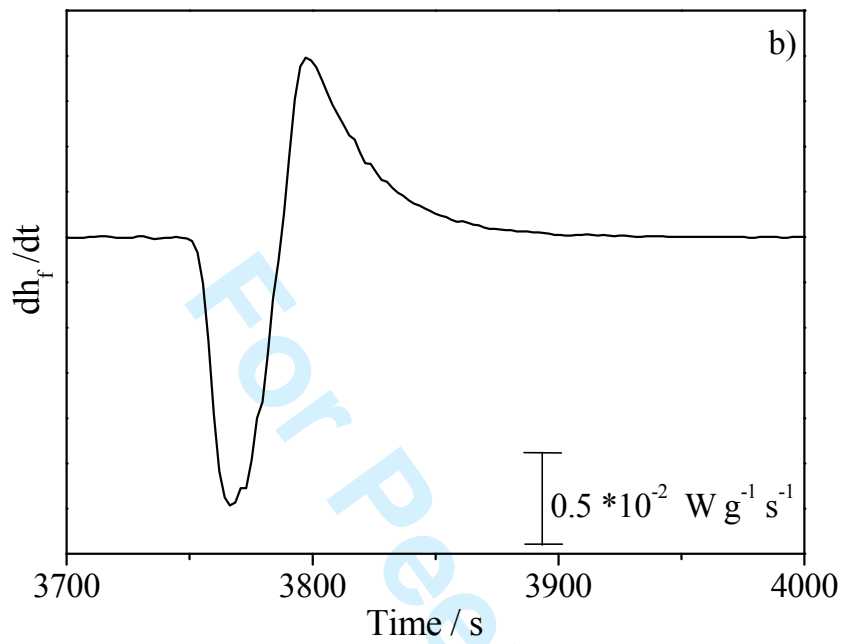


Figure 7a

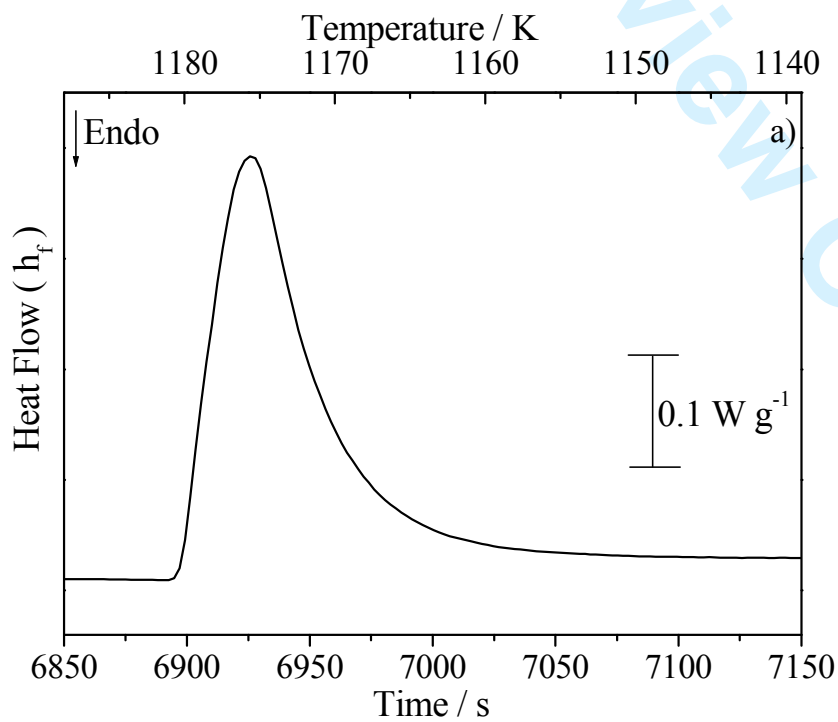


Figure 7b

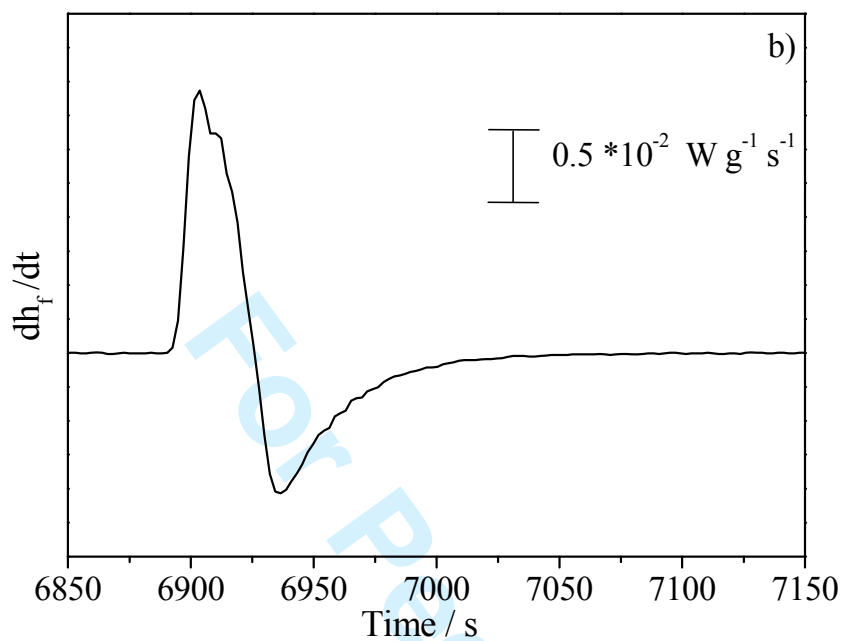


Figure 8a

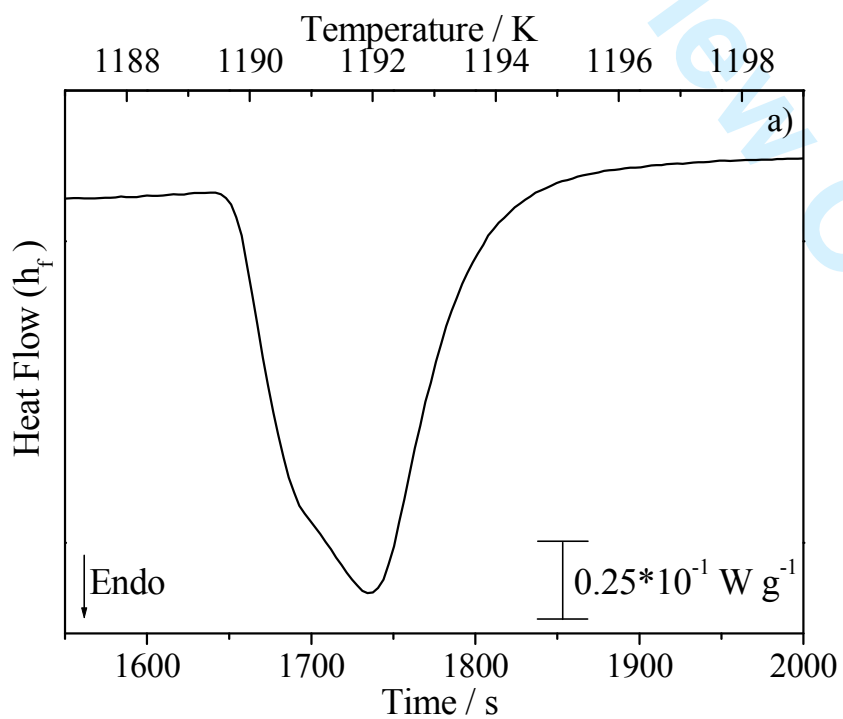


Figure 8b

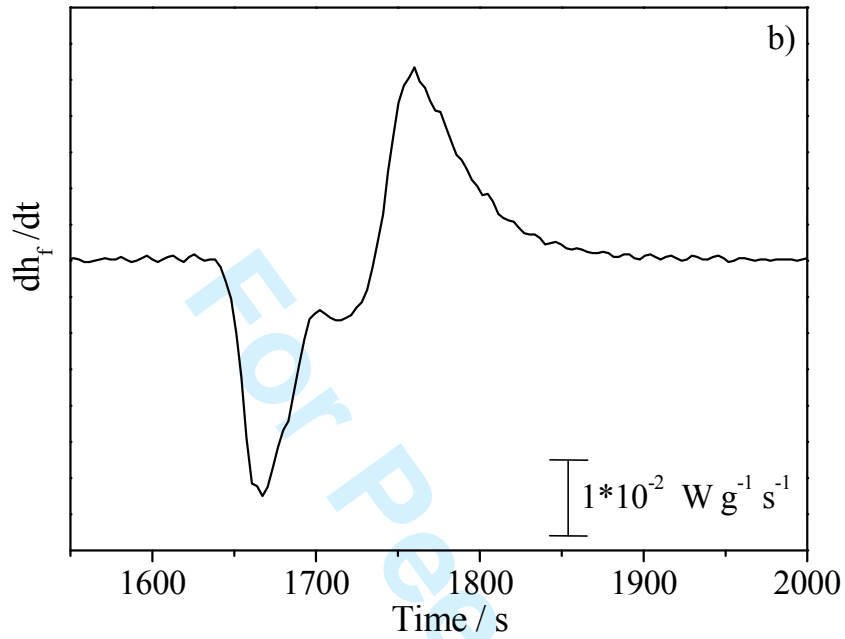


Figure 9a

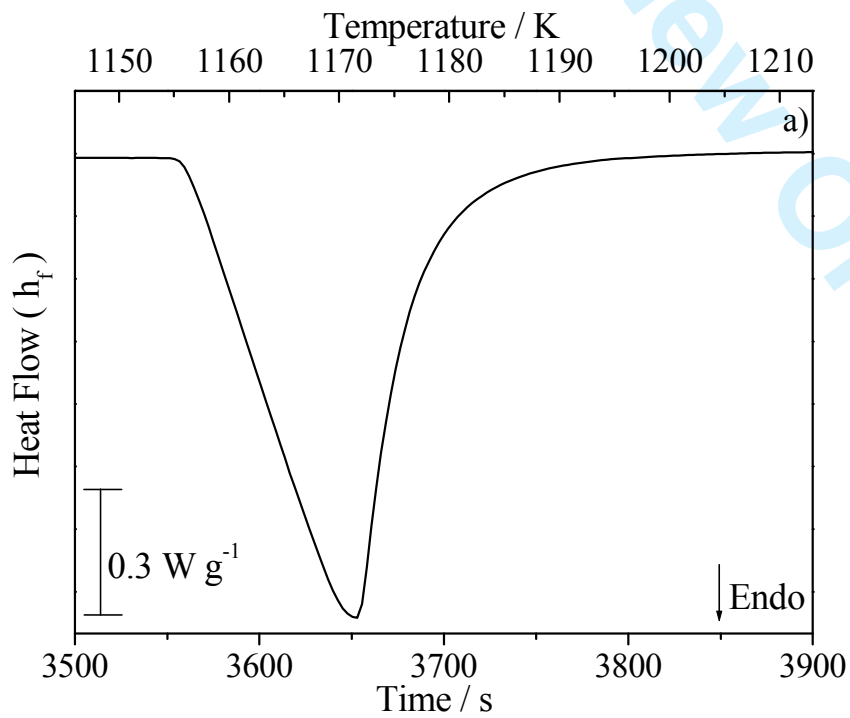


Figure 9b

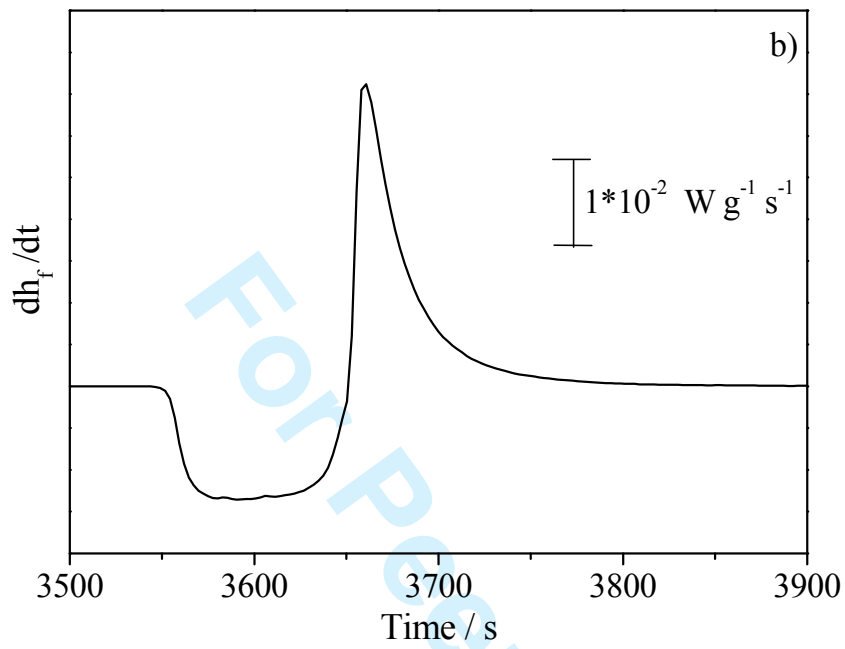


Figure 10a

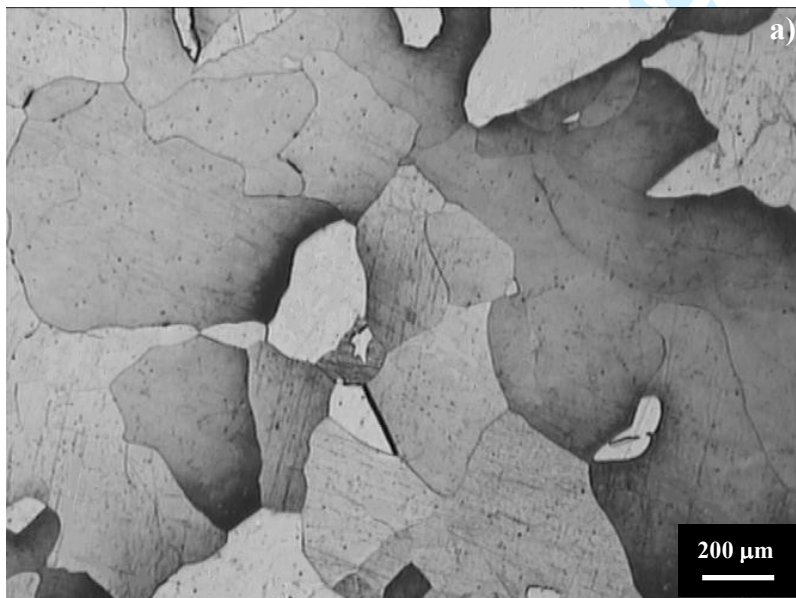


Figure 10b

